Alkenone isotopes show evidence of active carbon concentrating mechanisms in coccolithophores as aqueous carbon dioxide concentrations fall below 7 $\mu mol L^{-1}$

Marcus P. S. Badger[1]

[1]School of Environment, Earth & Ecosystem Sciences, The Open University, Milton Keynes, MK7 6AA, UK

Correspondence: Marcus P. S. Badger (marcus.badger@open.ac.uk)

Abstract.

Coccolithophores and other haptophyte algae acquire the carbon required for metabolic processes from the water in which they live. Whether carbon is actively moved across the cell membrane via a carbon concentrating mechanism, or passively through diffusion, is important for haptophyte biochemistry. The possible utilisation of carbon concentrating mechanisms also has the potential to over-print one proxy method by which ancient atmospheric CO_2 concentration is reconstructed using alkenone isotopes. Here I show that carbon concentrating mechanisms are likely used when aqueous carbon dioxide concentrations are below 7 $\mu mol L^{-1}$. I compile published alkenone based CO_2 reconstructions from multiple sites over the Pleistocene and recalculate them using a common methodology, which allows comparison to be made with ice core CO_2 records. Interrogating these records reveal that the relationship between proxy- and ice core- CO_2 breaks down when local aqueous CO_2 concentration falls below 7 $\mu mol L^{-1}$. The recognition of this threshold explains why many alkenone based CO_2 records fail to accurately replicate ice core CO_2 records, and suggests the alkenone proxy is likely robust for much of the Cenozoic when this threshold was unlikely to be reached in much of the global ocean.

1 Introduction

Alkenones are long–chain (C_{37-39}) ethyl– and methy– ketones (Figure 1; Brassell et al. (1986); Rechka and Maxwell (1987)) produced by a restricted group of photosynthetic haptophyte algae (Conte et al., 1994). Produced by a narrow group of organisms which live exclusively in the photic zone, alkenones allow probing of algal biogeochemistry, and as alkenones are often preserved in the sedimentary record, alkenones can also provide information about past environmental conditions.

Two main proxy systems based on alkenone geochemistry exist, one allows reconstruction of sea surface temperature (SST) and relies on the changing degree of unsaturation of the C_{37} alkenone ($U^{K'}_{37}$) (Brassell et al., 1986) whilst a second for atmospheric CO_2 concentration is based on reconstructing the isotopic fractionation which takes place during photosynthesis (ε_p) (Laws et al., 1995; Bidigare et al., 1997). It is the second system using the stable carbon isotopic composition of the preserved

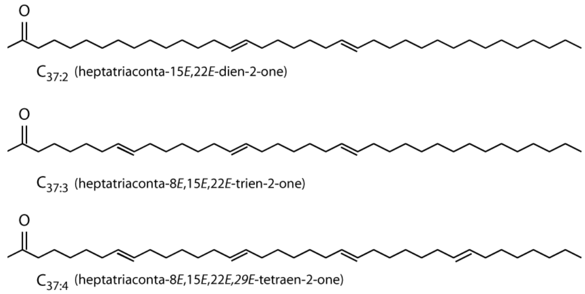

Figure 1. Alkenones are C_{37} unsaturated methyl ketones (Brassell et al., 1986; Rechka and Maxwell, 1987).

alkenones for reconstructing atmospheric $\mathrm{CO_2}$ concentration (referred to throughout as $\mathrm{CO}_{2(\varepsilon_\mathrm{p}-\mathrm{alk})}$) which is the focus of this study.

In the modern ocean alkenones are produced primarily by two dominant coccolithophore species; *Emiliania huxleyi* and *Gephyrocapsa oceanica*. *E. huxleyi* first appeared 290 kyr ago, and began to dominate over *G. oceanica* around 82 kyrs ago (Gradstein et al., 2012; Raffi et al., 2006). However alkenones are commonly found in sediments throughout the Cenozoic, with the oldest reported detections from mid-Albian aged black shales (Farrimond et al., 1986). Prior to the evolution of *G. oceanica* alkenones were most likely produced by other closely related species from the Noelaerhabdaceae family (Marlowe et al., 1990; Volkman, 2000). Micropaleontological and molecular data split the coccolith-bearing haptophytes into two distinct phylogenetic clades; the Isochrysidales and Coccolithales. The Isochrysidales contain the modern alkenone producing taxa including *E. huxleyi* and *G. oceanica*, and fossil reticulofenestrids. Meanwhile the non-alkeone producers are separated into the order Coccolithales which includes *Coccolithus pelagicus* and *Calcidiscus leptoporus* along with most other coccolithophores.

Proxies for atmospheric $\mathrm{CO_2}$ concentration including $\mathrm{CO}_{2(\varepsilon_\mathrm{p}-\mathrm{alk})}$, those based on the $\delta^{11}\mathrm{B}$ of planktic foraminifera, geochemical modelling and stomatal density, broadly agree that over the Cenozoic atmospheric $p\mathrm{CO_2}$ declined from high levels (>1000 $\mathrm{\mu atm}$) in the "greenhouse" worlds of the Paleocene and Eocene to close to modern day values (around 400 $\mathrm{\mu atm}$) in the Pliocene (Pagani et al., 2005, 2011; Pearson et al., 2009; Anagnostou et al., 2016; Foster et al., 2017; Sosdian et al., 2018; Super et al., 2018; Zhang et al., 2013; Beerling and Royer, 2011). However, recently discrepencies have emerged between $\mathrm{CO}_{2(\varepsilon_\mathrm{p}-\mathrm{alk})}$ and other $\mathrm{CO_2}$ proxies at the <400 $\mathrm{\mu atm}$ atmospheric $\mathrm{CO_2}$ concentrations of the Pleistocene (i.e. Badger et al. (2019, 2013a) and compare Badger et al. (2013b) and Pagani et al. (2009) with Martínez-Botí et al. (2015)). Whilst the long-standing differences between alkenone (Pagani et al., 1999), $\delta^{11}\mathrm{B}$ (Foster et al., 2012) and stomatal proxies (Kürschner et al., 2008) in the Miocene $\mathrm{CO_2}$ reconstructions have been partially resolved with new SST records (Super et al., 2018), differences remain in the Pliocene (Pagani et al., 2009; Badger et al., 2013b; Martínez-Botí et al., 2015) and Pleistocene (Badger et al., 2019).

1.1 Carbon Concentrating mechanisms

One plausible reason for the discrepancies between $CO_{2(\varepsilon_p-\mathrm{alk})}$ and other proxies for atmospheric CO_2 is the operation of active carbon concentrating mechanisms (CCMs) in haptophytes. These are potentially important as $CO_{2(\varepsilon_p-\mathrm{alk})}$ assumes purely passive uptake of carbon into the haptophyte cell purely via diffusion (Laws et al., 1995; Bidigare et al., 1997). The potential for CCMs to effect $CO_{2(\varepsilon_p-\mathrm{alk})}$ has long been known (Laws et al., 1997, 2002; Cassar et al., 2006) and recent work has refocussed efforts on understanding CCMs in $CO_{2(\varepsilon_p-\mathrm{alk})}$ (Bolton et al., 2012; Bolton and Stoll, 2013; Stoll et al., 2019; Zhang et al., 2019, 2020). Coccolithophores are thought to have low efficiency CCMs, especially compared to diatoms, dinoflagellates and *Phaeocystis*, with evidence that CCMs play a minor role in coccolithophore biochemistry in the CO_2 replete worlds of the early Cenozoic (Bolton et al., 2012; Reinfelder, 2011). Direct evidence from experimentation with the marine diatom *Phaeodactylum tricornutum* suggest that both passive diffusive uptake and active CCMs operate at the same time, with active uptake used to moderate internal cell CO_2 concentrations to minimise energy use during transport to carboxylation sites (Laws et al., 1997). CO_2, unlike some other nutrients, is replete within the water column, especially when considering the DIC reservoir which includes bicarbonate (HCO_3^-), carbonate (CO_3^{2-}) and dissolved CO_2 ($[CO_2]_{(aq)}$) . However, due to the relatively slow diffusion of dissolved $[CO_2]_{(aq)}$ through water and the slow kinetics of the bicarbonate to $[CO_2]_{(aq)}$ transformation, surface water $[CO_2]_{(aq)}$ can still be depleted by photosynthetic activity. This can become particularly problematic in species which form blooms, and at the cell boundary of species with limited motility. It should be no surprise therefore that many marine photosynthetic organisms have evolved with mechanisms to concentrate carbon within the cell.

The enzyme carbonic anhydrase (CA) can catalyse the dehydration of HCO_3^- to $[CO_2]_{(aq)}$ to speed up availability of carbon if the $[CO_2]_{(aq)}$ reservoir is depleted and has been observed in several haptophytes including coccolithophores (Rost et al., 2003; Riebesell et al., 2007). The exact contribution of CA remains unclear but two possible mechanisms for CCMs have been postulated (Reinfelder, 2011) (1) CA catalyzes dehydration of HCO_3^- at the cell surface, which then allows increased CO_2 to diffuse into the cell passively and (2) HCO_3^- is transported into the cell and then converted by CA. Both of these options will likely impact the $CO_{2(\varepsilon_p-\mathrm{alk})}$ proxy, firstly by changing the effective $[CO_2]_{(aq)}$ within the cell (and so impacting ε_p), and secondly by imparting another carbon isotopic fractionation during CA catalyzation which is not considered by the $CO_{2(\varepsilon_p-\mathrm{alk})}$ proxy system. However CA activity in coccolithophores does not appear to be regulated by CO_2 as it is in diatoms and *Phaeocystis* (Rost et al., 2003) which may indicate a less well developed CCM in coccolithophores.

Calcifying coccolithophores (which include alkenone producers *E. huxleyi* and *G. oceanica*) may be able to utilize HCO_3^- directly as a carbon source (Trimborn et al., 2007), with precipitation of $CaCO_3$ providing an acid for the dehydration of HCO_3^- but this still requires sufficent HCO_3^- entering the cell and it is unclear whether calcification aids DIC acquisition (Riebesell et al., 2000; Zondervan et al., 2002). The light dependant leak of carbon (as CO_2 and DIC) back from haptophyte cells (including the coccolithophore *E. huxleyi*) to seawater (Tchernov et al., 2003) suggests that CCMs are energy intensive and can concentrate DIC within the cell. Even with active CCMs, it appears that in the ocean coccolithophores are CO_2 limited under some circumstances (Riebesell et al., 2007).

Table 1. Sites with Pleistocene $CO_{2(\varepsilon_p-alk)}$ records. Note that the MANOP Site C record was generated to track changes in surface water–atmosphere equilibrium not atmospheric pCO_2, so although included here for completeness, is not included in the analysis. Distance from coast is calculated from the intermediate resolution version of GSHHG and computed using Generic Mapping Tools (GMT) (Wessel and Smith, 1996; Wessel et al., 2019)

Site	Age interval (kyr)	Latitude	Longitude	Water depth (m)	Distance from coast (km)	Reference
05PC-21	0.5–188	38° 24'N	131° 33'E	1721	108	Bae et al. (2015)
DSDP 619	3–92	27° 11.61' N	91° 24.54' W	2259	489	Jasper and Hayes (1990)
NIOP 464	7.8–29	22° 9' N	63° 21'E	1470	333	Palmer et al. (2010)
ODP 999	111–258	12° 44.639' N	78° 44.360' W	2839	249	Badger et al. (2019)
ODP 925	20–580	4° 12.249' N	43° 29.334' W	3042	626	Zhang et al. (2013)
MANOP Site C	0.8–253	0° 57.2" N	138° 57.3' W	4287	998	Jasper et al. (1994)
GeoB 1016-3	1.3–196	11° 46.2' S	11° 40.9' E	3410	185	Andersen et al. (1999)

*The full record for ODP Site 925 extends to 38.62 Ma

2 Materials and Methods

2.1 Calculating $\mathbf{CO_2}$ from alkenone δ^{13}C values: The $\mathbf{CO_{2(\varepsilon_p-alk)}}$ proxy

In this study I use the now large number of published $CO_{2(\varepsilon_p-alk)}$ records which overlap with ice core records of atmospheric CO_2 concentration (Tables 1 & 2) to explore the relationship between $CO_{2(\varepsilon_p-alk)}$ and CCMs in the Pleistocene, where our understanding of atmospheric CO_2 concentration is best.

Multiple records of $CO_{2(\varepsilon_p-alk)}$ have been published for the Pleistocene (Figure 2, Table 1) allowing direct comparision with ice core based CO_2 records (Table 2). These records are globally distributed in longitude, but are concentrated at low latitude sites, largely as there is a general preference for sites which have (in the modern ocean) surface waters close to equilibrium with the atmosphere (Figure 2, Table 1). In longer term palaeoclimate studies there has also been a preference for low latitude, gyre sites in the belief that these sites are more likely to be oceanographically stable over long time intervals (Pagani et al., 1999). Most of the records included here (Table 1, Figure 2) were generated with the aim to reconstruct atmospheric CO_2 concentration, however one, the MANOP C Site of Jasper et al. (1994), was used to explicitly reconstruct changing disequilibrium due to oceanographic frontal changes over time, and so is excluded from the following analysis.

Whilst these sites do only span a relatively small latitudinal extent, the diversity of settings does allow for investigation of any secondary controls on alkenone δ^{13}C values ($\delta^{13}C_{alkenone}$). In particular, differences in oceanographic setting and SST to test the hypothesis that low $[CO_2]_{(aq)}$ breaks the relationship between $\delta^{13}C_{alkenone}$ and atmospheric CO_2 concentration, as might be expected if haptophytes are able to actively take up carbon from seawater to meet metabolic demand – i.e. activate CCMs.

Table 2. Sources of ice core data, as compiled by Bereiter et al. (2015). WAIS - West Antarctic Ice Sheet, TALDICE - TALos Dome Ice CorE, EDML - EPICA Dronning Maud Land

Age interval (kyr)	Ice core location	Reference
-0.051–1.8	Law Dome	Rubino et al. (2013)
1.8–2	Law Dome	MacFarling Meure et al. (2006)
2–11	Dome C	Monnin et al. (2001, 2004)
11–22	WAIS	Marcott et al. (2014)
22–40	Siple Dome	Ahn and Brook (2014)
40–60	TALDICE	Bereiter et al. (2012)
60–115	EDML	Bereiter et al. (2012)
105–155	Dome C Sublimation	Schneider et al. (2013)
155–393	Vostok	Petit et al. (1999)

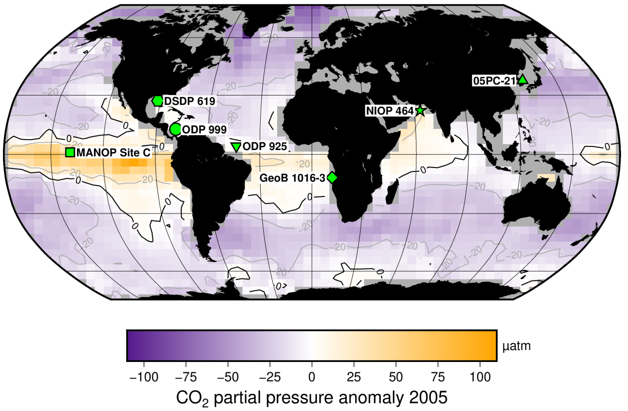

Figure 2. Study sites relative to mean annual surface ocean CO_2 disequilibrium for 2005. Sites are globally distributed in longitude but restricted in latitude, as generally sites are chosen to be close to surface water equilibrium with the atmosphere. Sites used for this study are indicated, over the mean annual surface ocean disequilibrium for 2005 calculated from Takahashi et al. (2014). The MANOP C Site (Jasper et al., 1994) was choosen to study the disequilbrium at that site, so is shown here but not used in the following analyses. Site symbols are used throughout the figures: ODP 999 - circle, 05PC-21 - triangle, ODP 925 - inverted triangle, DSDP 619 - hexagon, MANOP Site C - square, NIOP 464 - star, GeoB 1016-3 - diamond.

To facilitate fair comparision between sites and consistent comparision with the ice core records, all $CO_{2(\varepsilon_p-\mathrm{alk})}$ records were recalculated using a consistent approach. The approach is based on Bidigare et al. (1997) which updated the initial approach of Jasper and Hayes (1990) to $CO_{2(\varepsilon_p-\mathrm{alk})}$. This approach removes some additional corrections used in the original publication of the records (such as growth rate adjustment for NIOP 464 (Palmer et al., 2010)) but does allow for direct comparison to be made. For all sites the 'b' term was estimated using modern day surface $[\mathrm{PO_4^{3-}}]$ (Bidigare et al., 1997; Pagani et al., 2009)

An overview of how $\mathrm{CO_{2(\varepsilon_p - alk)}}$ data are typically generated is given in Badger et al. (2013b). Briefly, to calculate ε_p requires the stable carbon isotopic composition of the dissolved $\mathrm{CO_2}$ ($\delta^{13}\mathrm{C_{CO_{2(aq)}}}$) and haptophyte biomass ($\delta^{13}\mathrm{C_{org}}$). The isotopic fractionation between $\delta^{13}\mathrm{C_{alkenone}}$ and $\delta^{13}\mathrm{C_{org}}$ is first corrected assuming a constant fractionation ($\varepsilon_\mathrm{alkenone}$) of 4.2 ‰ (Garcia et al., 2013; Popp et al., 1998; Bidigare et al., 1997):

$$\varepsilon_\mathrm{alkenone} = \frac{\delta^{13}C_{alkenone} + 1000}{\delta^{13}C_{org} + 1000} - 1 \tag{1}$$

The isotopic composition of dissolved inorganic carbon (DIC) is estimated using (ideally) the $\delta^{13}\mathrm{C}$ value of planktic foraminifera and the temperature-dependant fractionation between calcite and $[\mathrm{CO_2}]_\mathrm{(g)}$ experimentally determined by Romanek et al. (1992), where T is sea surface temperature in degrees Celsius (SST):

$$\varepsilon_{calcite-CO_{2(g)}} = 11.98 - 0.12T \tag{2}$$

The value the carbon isotopic composition of $\mathrm{CO_{2(g)}}$ ($\delta^{13}\mathrm{C_{CO_{2(g)}}}$) can then be calculated:

$$\delta^{13}C_{CO_{2(g)}} = \frac{\delta^{13}C_{carbonate} + 1000}{\varepsilon_{calcite-CO_{2(g)}}/1000 + 1} - 1000 \tag{3}$$

From this $\delta^{13}\mathrm{C_{CO_{2(aq)}}}$ can be calculated using the relationship experimentally determined by Mook et al. (1974):

$$\varepsilon_{CO_{2(aq)}-CO_{2(g)}} = \frac{-373}{T + 273.15} + 0.19 \tag{4}$$

and

$$\begin{aligned}\delta^{13}C_{CO_{2(aq)}} = &\Big(\frac{\varepsilon_{CO_{2(aq)}-CO_{2(g)}}}{1000} + 1\Big)\\ &.\big(\delta^{13}C_{CO_{c(g)}} + 1000\big)\\ &- 1000\end{aligned} \tag{5}$$

Finally ε_p can be calculated:

$$\varepsilon_p = \left(\frac{\delta^{13}C_{CO_{2(aq)}} + 1000}{\delta^{13}C_{org} + 1000} - 1\right).1000 \tag{6}$$

and from that $[\mathrm{CO_2}]_\mathrm{(aq)}$ is calculated using the isotopic fractionation during carbon fixation (ε_f) and 'b', which represents the summation of physiological factors:

$$[CO_2]_{(aq)} = \frac{b}{\varepsilon_f - \varepsilon_p} \tag{7}$$

Here ε_f is assumed to be a constant 25 ‰ (Bidigare et al., 1997). In the modern ocean the 'b' term, which accounts for physiological factors such as cell size and growth rate, shows a close correlation with $[\mathrm{PO}_4^{3-}]$ (Bidigare et al., 1997; Pagani et al., 2009). However, the relationship between b, growth rate and $[\mathrm{PO}_4^{3-}]$ has recently been questioned (Zhang et al., 2019, 2020) but for the purposes of this analysis is assumed to hold. This is discussed further below. Values for SST, $\delta^{13}\mathrm{C}_\mathrm{alkenone}$, $\delta^{13}\mathrm{C}_\mathrm{carbonate}$, salinity and $[\mathrm{PO}_4^{3-}]$ are either taken from the original publications or estimated from modern ocean estimates (Takahashi et al., 2009; Antonov et al., 2010; Garcia et al., 2013; Locarnini et al., 2013).

Providing that the atmosphere is in equilibrium with surface water, the concentration of atmospheric $\mathrm{CO_2}$ can be calculated from $[\mathrm{CO_2}]_\mathrm{(aq)}$, (and vice versa if atmospheric $\mathrm{CO_2}$ concentration is known) using Henry's law:

$$pCO_2 = \frac{[CO_2]_{(aq)}}{K_\mathrm{H}} \tag{8}$$

The solubility coefficient ($\mathrm{K_H}$) is dependant on salinity and SST, and here is calculated following the parameterization of Weiss (1970, 1974).

3 Results

3.1 Multi-site comparisons between $\mathbf{CO_{2(\varepsilon_p - alk)}}$ and the ice core records

Across the six sites included in this analysis, there are 217 $\mathrm{CO}_{2(\varepsilon_\mathrm{p}-\mathrm{alk})}$-based estimates of atmospheric $\mathrm{CO_2}$ concentration over the past 260 Ka for comparison with the ice core records (Table 2; Bereiter et al. (2015)). When all $\mathrm{CO}_{2(\varepsilon_\mathrm{p}-\mathrm{alk})}$ estimates are considered together over 260 Ka, this compilation of proxy-based records fails to replicate the ice core record (Figure 3). This has already been noted at specific sites (e.g. Site 999 in the Caribbean Badger et al. (2019)) but this is the first time that all available records coincident with the Pleistocene ice core records have been compiled using a common methodology. Notably the $\mathrm{CO}_{2(\varepsilon_\mathrm{p}-\mathrm{alk})}$ based estimates are rarely lower than time-equivalent ice core estimate, but frequently higher. Given that haptophytes require carbon to satisfy metabolic demand, this is perhaps unsurprising; if at times of low carbon availability haptophytes can switch from passive to active uptake to satisfy metabolic demand, it would be times of low atmospheric $\mathrm{CO_2}$ concentration (and so lower $[CO_2]_{(aq)}$) when the active uptake is most likely to be needed. As $\mathrm{CO}_{2(\varepsilon_\mathrm{p}-\mathrm{alk})}$-based estimates of atmospheric $\mathrm{CO_2}$ concentration rely on the assumption of a purely diffusive uptake of carbon, it is therefore likely that the proxy would perform worse at times of low atmospheric $\mathrm{CO_2}$ concentration.

The haptophytes do not directly interact with the atmosphere, obtaining their carbon from dissolved carbon. As it is not only atmospheric $\mathrm{CO_2}$ concentration which controls the concentration of dissolved carbon ($[\mathrm{CO_2}]_\mathrm{(aq)}$), but also temperature, alkalinity and other oceanographic factors which control the equilibrium state between surface waters at the atmosphere, (Figure 2) the multiple sites in different settings now give the opportunity to test whether other factors are important in controlling the accuracy of $\mathrm{CO}_{2(\varepsilon_\mathrm{p}-\mathrm{alk})}$.

To produce time-equilvalent estimates of atmospheric $\mathrm{CO_2}$ concentration for comparison with the ice core records, a simple linear interpolation of the Bereiter et al. (2015) compilation was initially used (Figure 4). This assumes that both the age model

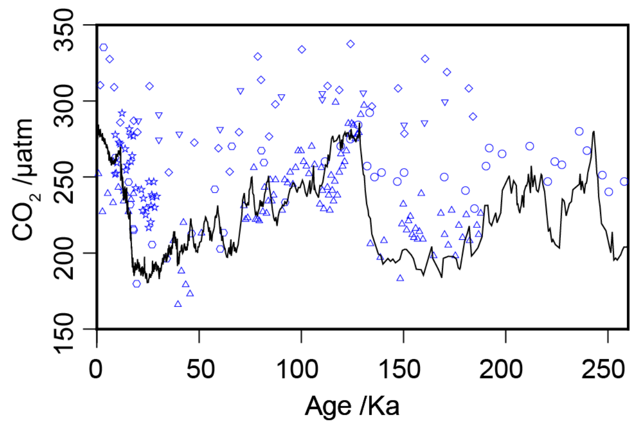

Figure 3. Compiled $CO_{2(\varepsilon_p-\mathrm{alk})}$-based estimates of atmospheric CO_2 concentration over the past 260 Ka (blue circles), with the ice core compilation of Bereiter et al. (2015) shown as the solid black line. Full sources for the ice core and $CO_{2(\varepsilon_p-\mathrm{alk})}$ records are in Tables 1 and 2.

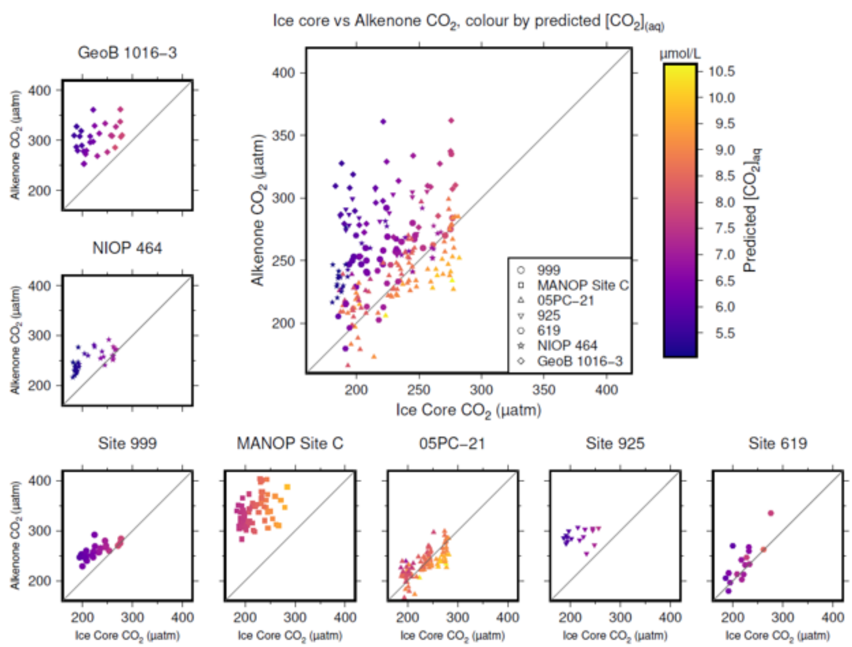

Figure 4. Crossplots of $CO_{2(\varepsilon_p-\mathrm{alk})}$-based atmospheric CO_2 concentration (y-axes) vs the time-equivalent estimate from ice core records (x-axes; Bereiter et al. (2015); Table 2)). The large panel compiles all sites, with the exception of MANOP Site C, as explained in the text. Symbols are coloured by predicted $[CO_2]_{(aq)}$ for each site and time as explained in the text. Full sources for alkenone data are shown in Table 1. A 1:1 line is included in all plots for comparison.

of the ice core and the published age models of the sites are correct and equivalent. This is almost certainly not the case, and so for the calculations below, a $\pm$3000 year uncertainty is included for ages of both the ice core and $CO_{2(\varepsilon_p-alk)}$ values. Figure 4 shows that $CO_{2(\varepsilon_p-alk)}$-based atmospheric CO_2 concentration agree with ice core CO_2 at some sites and at some times, but not throughout. Sites 05-PC21 (Bae et al., 2015) and DSDP Site 619 (Jasper and Hayes, 1990) perform quite well, throughout, whilst ODP Site 999 (Badger et al., 2019) and NIOP 464 (Palmer et al., 2010) only appear to agree at higher values of CO_2, at ODP Site 925 (Zhang et al., 2013) and GEoB 1016-3 (Andersen et al., 1999) there is very little overlap between the two methods of reconstructing atmospheric CO_2 concentration.

To explore whether $[CO_2]_{(aq)}$ is an imporant influence on $CO_{2(\varepsilon_p-alk)}$, I calculate predicted $[CO_2]_{(aq)}$ ($[CO_2]_{(aq)-predicted}$) for each of the samples. To calculate $[CO_2]_{(aq)-predicted}$, the time-equivalent value of atmospheric CO_2 concentration from the ice core record is used in combination with Eq. 8 to calculate $[CO_2]_{(aq)}$ at the time of alkenone production for each sample. Reconstructed estimates of SST and salinity are used as for $CO_{2(\varepsilon_p-alk)}$ above, along with any estimated surface water-atmosphere disequilbrium. Points in Figure 4 are then coloured by $[CO_2]_{(aq)-predicted}$.

Inspection of Figure 4 suggests a connection between ($[CO_2]_{(aq)-predicted}$) and the skill of $CO_{2(\varepsilon_p-alk)}$ to reconstruct atmospheric CO_2 concentration. The points clustering around the 1:1 line are lighter in colour (so with higher $[CO_2]_{(aq)-predicted}$), whilst points falling away from the 1:1 line have lower $[CO_2]_{(aq)-predicted}$. To explore this relationship, I progressively restricted the included samples on the basis of $[CO_2]_{(aq)-predicted}$, and at each stage calculated a Pearson correlation co-efficient (r) and coefficient of determination (r^2) for each subset. Under this analysis the correlation progressively increased as more of the low $[CO_2]_{(aq)-predicted}$ samples were excluded (Figure 5). All analyses were performed in R (R Core Team, 2020) using RStudio (RStudio Team, 2020). This suggests that the fidelity of the $CO_{2(\varepsilon_p-alk)}$ depends on the concentration of $[CO_2]_{(aq)}$, improving at higher levels of $[CO_2]_{(aq)}$.

To further investigate this potential relationship, I progressively exclude samples based on $[CO_2]_{(aq)-predicted}$ with a step size of 0.05 $\mu molL^{-1}$, again calculating Pearson correlation coefficients and coefficients of determination between ice core and $CO_{2(\varepsilon_p-alk)}$ for each subsample of the population. The result is shown in Figure 6. Here the analysis shows, similar to Figure 5, that as the samples with lowest $[CO_2]_{(aq)-predicted}$ are progressively removed, the correlation between ice core and $CO_{2(\varepsilon_p-alk)}$ increases. Furthermore, this continues only up until $[CO_2]_{(aq)-predicted}$ reaches 7 $\mu molL^{-1}$. Above this, the coefficient of determination plateaus, until the subsample reaches such a small size that spurious correlations become important (Figure 6b).

3.2 Sensitivity and Uncertainty Tests

It is possible that the pattern seen in Figure 6b could emerge from a dataset shaped with increasing densisity surrounding the 1:1 correlation line without being driven by changes in $[CO_2]_{(aq)-predicted}$. To explore this possiblity I ran a series of sensitivity experiments. In these, rather than reducing the sample by filtering by $[CO_2]_{(aq)-predicted}$, the whole dataset (Table 1) was randomly ordered, and then stepwise subsampled. To make this equivalent to the $[CO_2]_{(aq)-predicted}$ analysis above, I set the size of each subsample to be equal to each step in the original analysis. This produces a randomly selected, but same sized sub-sample such that the size of the subsample reduces in the same way as shown in Figure 6b). Pearson correlation

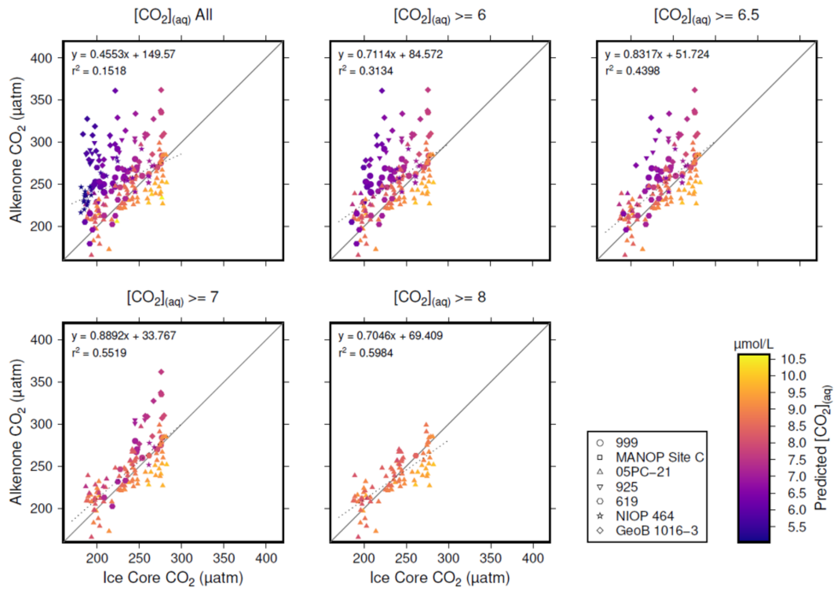

Figure 5. Crossplots of $CO_{2(\varepsilon_p-\mathrm{alk})}$-based atmospheric CO_2 concentration (Table 1; y-axes) vs the time-equivalent estimate from ice core records (x-axes; Bereiter et al. (2015); Table 2)). The sample of published vales of $CO_{2(\varepsilon_p-\mathrm{alk})}$ was progressively restricted by $[CO_2]_{(aq)-\mathrm{predicted}}$, indicated by the subplot titles. Individual values are coloured by $[CO_2]_{(aq)-\mathrm{predicted}}$, and Sites indicated by shape (see key). Coefficients of determination and equations of best fit are shown in each panel, along with a 1:1 line.

coefficients and coefficients of determination were calculated for each subsample as above, and I repeated this 1000 times, with the order of each sample randomized each time.

To allow for possible age model uncertainties, a 3000 year (1σ) uncertainty was also applied to each sample. This uncertainty was applied to the age of each sample prior to sampling of the ice core record, and is applied as a normally distributed uncertainty. Uncertainty in $CO_{2(\varepsilon_p-\mathrm{alk})}$ measurements is typically calculated using Monte Carlo modelling of all the parameters (i.e Pagani et al. (1999); Badger et al. (2013a, b)), however this was not done in all the published work (Table 1), and some differences in approach were found across the published work. Therefore to create $CO_{2(\varepsilon_p-\mathrm{alk})}$ uncertainty estimates for each value in this study, I emulate the uncertainties based on the $CO_{2(\varepsilon_p-\mathrm{alk})}$ value. I built a simple emulator (Figure 7) by running Monte Carlo uncertainty estimates for all of the included datasets (Table 1) using the same estimates of uncertainty for each variable in the $CO_{2(\varepsilon_p-\mathrm{alk})}$ calculation as applied in Badger et al. (2013a, b). This then allows the uncertainty to be included in the $[CO_2]_{(aq)-\mathrm{predicted}}$ calcuation as well as $CO_{2(\varepsilon_p-\mathrm{alk})}$, and allowed for uncertainty estimates to be site-ambivalent.

The result is shown in Figure 6c,d, and suggests that the 7 $\mu\mathrm{molL}^{-1}$ break point remains valid. The absolute value of r^2 is reduced, even at higher $[CO_2]_{(aq)-\mathrm{predicted}}$, but this would be expected given the addition of uncertainty in age model, as the published age is most likely to align with the ice core. Given the rapid rate of change at deglaciations, this effect is likely to be particularly pronounced in this dataset as many records have high temporal resolution around deglaciations in order to attempt

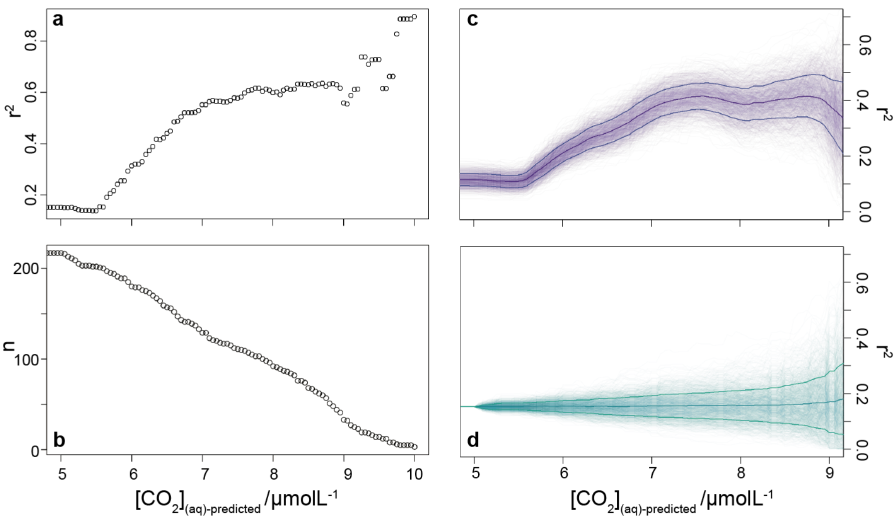

Figure 6. Coefficient of determination (panel a) of a reducing sample of all compiled $CO_{2(\varepsilon_p-\mathrm{alk})}$ (Table 1) vs the time-equivalent estimate from ice core records (Bereiter et al. (2015); Table 2). The sample reduces stepwise by 0.05 $\mu\mathrm{molL}^{-1}$, and the number of records in each subsample is shown in panel b. Panel c shows a 1000 member Monte Carlo analysis, whereby uncertainty in $CO_{2(\varepsilon_p-\mathrm{alk})}$ and age is considered, as detailed in the text. Panel d shows a similar 1000 member Monte Carlo analysis, but with random sampling of the whole $CO_{2(\varepsilon_p-\mathrm{alk})}$ population so that the number of samples is equivalent to the dataset shown in panel c, ie the size of the sample follows that shown panel b. Means and one σ uncertainties are shown as the bold lines.

to resolve them. Any small age model offset introduced by the error modelling in these intervals also clearly has the potential to induce large differences between the $CO_{2(\varepsilon_p-\mathrm{alk})}$ and ice core values. Figure 6c,d clearly demonstrates that it is the filtering by $[CO_2]_{(\mathrm{aq})-\mathrm{predicted}}$ rather than any spurious correlations which determine the shape of the data in Figure 6a.

4 Discussion

The plateau in r^2 in Figures 6a and 6c suggest that below a $[CO_2]_{(\mathrm{aq})-\mathrm{predicted}}$ of ~ 7 $\mu\mathrm{molL}^{-1}$ $CO_{2(\varepsilon_p-\mathrm{alk})}$ is no longer as good a predictor of ice core CO_2 as when $[CO_2]_{(\mathrm{aq})-\mathrm{predicted}} > 7$ $\mu\mathrm{molL}^{-1}$. This is clear from comparing the relationship between samples where $[CO_2]_{(\mathrm{aq})-\mathrm{predicted}} < 7$ $\mu\mathrm{molL}^{-1}$ with those where $[CO_2]_{(\mathrm{aq})-\mathrm{predicted}} > 7$ $\mu\mathrm{molL}^{-1}$ in Figure 8. Here the r^2 for the former of 0.15 is substantially less than the latter of 0.55. I suggest that this is because below this threshold, the fundamental assumption of $CO_{2(\varepsilon_p-\mathrm{alk})}$; that carbon is passively taken up by haptophytes, no longer holds true. One obvious explanation for why this would be the case is that at low levels of $[CO_2]_{(\mathrm{aq})}$ haptophytes have to rely more on active up take of carbon via CCMs in order to satisfy metabolic demand. Similar behaviour has been recognised in some culture studies (Laws et al., 1997, 2002; Cassar et al., 2006), with some evidence that the diatom *Phaeodactylum tricornutum* has a similar CCM threshold of 7 $\mu\mathrm{molL}^{-1}$ (Laws et al., 1997). Whilst the evidence for the mechanism of CCM is poorer for coccolithophores than

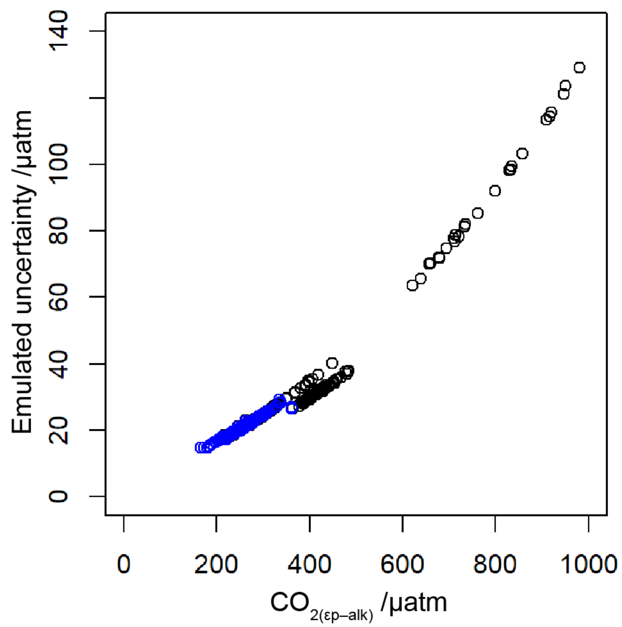

Figure 7. Emulated uncertainty in $CO_{2(\varepsilon_p-\mathrm{alk})}$, generated by running Monte Carlo uncertainty models for all sites in Table 1 applying the same approach to uncertainty as Badger et al. (2013a, b). Estimates used in this study are highlighted in blue.

it is for diatoms, any CCM would be expected to compromise the $CO_{2(\varepsilon_p-\mathrm{alk})}$ proxy, either by increased supply of $[CO_2]_{(\mathrm{aq})}$, further carbon isotopic fractionation effects during carbon transport or both (Stoll et al., 2019).

By applying a threshold value for $[CO_2]_{(\mathrm{aq})-\mathrm{predicted}}$ of 7 $\mu\mathrm{mol L}^{-1}$ to the published records (Table 1) values of $CO_{2(\varepsilon_p-\mathrm{alk})}$ which are influenced by active CCMs can be eliminated. Recognition of this new threshold value of $[CO_2]_{(\mathrm{aq})-\mathrm{predicted}}$ allows for a new record of Pleistocene $CO_{2(\varepsilon_p-\mathrm{alk})}$ to be compiled. This compilation then much better replicates the glacial-interglacial pattern of CO_2 change over the last 260 Ka (Figure 9). Whilst this present compilation does rely on ice core CO_2 records to estimate $[CO_2]_{(\mathrm{aq})-\mathrm{predicted}}$, and therefore has little direct utility as a CO_2 record, it does demonstrate that recognition of a threshold response allows accurate CO_2 reconstruction using $CO_{2(\varepsilon_p-\mathrm{alk})}$. This may represent the point at which isotopic effects of CCMs (plausibly through increased CA activity or HCO_3^- dehydration to meet C demand) overwhelms the assumptions of the $CO_{2(\varepsilon_p-\mathrm{alk})}$ proxy. This, and the behaviour shown in Figures 6a and 6c suggests that from the standpoint of the $CO_{2(\varepsilon_p-\mathrm{alk})}$ proxy CCMs may effectively be considered either active or not, and that when $[CO_2]_{(\mathrm{aq})}$ is plentiful passive uptake dominates, at least sufficiently in most oceanographic settings that $CO_{2(\varepsilon_p-\mathrm{alk})}$ can accurately record atmospheric CO_2 concentration. This implies that if areas of the ocean (or intervals of time) with low $[CO_2]_{(\mathrm{aq})}$ can be avoided, accurate reconstructions of atmospheric CO_2 concentration can be acquired using $CO_{2(\varepsilon_p-\mathrm{alk})}$.

As $[CO_2]_{(\mathrm{aq})}$ is effected by both SST via the temperature dependance of the Henry's law constant and atmospheric CO_2 concentration, for $CO_{2(\varepsilon_p-\mathrm{alk})}$ to be effective in reconstructing atmospheric CO_2 concentration, areas of warm water (i.e. tropical

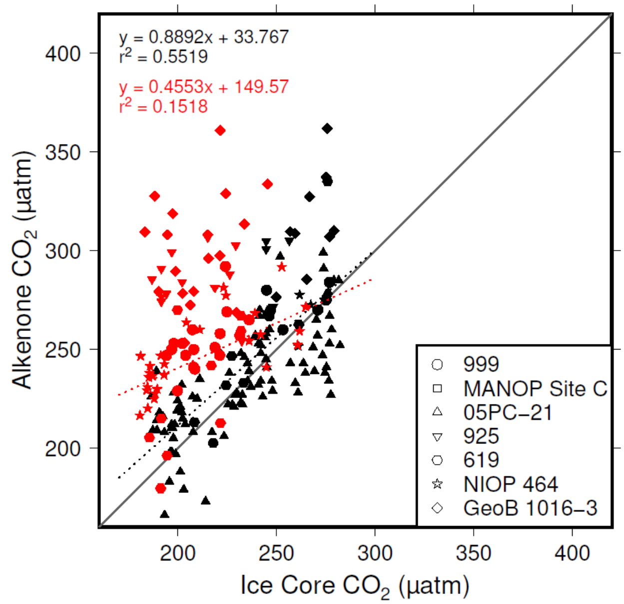

Figure 8. Correlations between $CO_{2(\varepsilon_p-\mathrm{alk})}$ and ice core CO_2 where $[CO_2]_{(aq)-\mathrm{predicted}}$ > 7 µmolL^{-1} (black symbols) and $[CO_2]_{(aq)-\mathrm{predicted}}$ < 7 µmolL^{-1} (red symbols).

or shallow shelf regions) under relatively low atmospheric CO_2 concentration must be avoided. However, as the atmospheric CO_2 control renders the global surface ocean sufficiently replete in $[CO_2]_{(aq)}$ at Pliocene-like levels of atmospheric CO_2 concentration and above (Martínez-Botí et al., 2015) at all but the warmest surface ocean temperatures, $CO_{2(\varepsilon_p-\mathrm{alk})}$ is likely to be a reliable system for most of the Cenozoic. It is only in the Pleistocene that atmospheric CO_2 concentration is low enough for CCMs to be widely active accross the surface ocean, with the low CO_2 glacials providing the most difficulty (Badger et al., 2019). This finding aligns well with evidence that CCMs developed in coccolithophores as a reponse to declining atmospheric CO_2 concentration through the Cenozoic, and were developing in $[CO_2]_{(aq)}$–limited parts of the ocean in the late Miocene at the earliest, and likely not widespread until the Plio-Pleistocene (Bolton et al., 2012; Bolton and Stoll, 2013).

There have been recent attempts to correct for CCMs in $CO_{2(\varepsilon_p-\mathrm{alk})}$-based reconstructions of atmospheric CO_2 concentration s (Zhang et al., 2019; Stoll et al., 2019; Zhang et al., 2020). However, these assume that CCMs are always active, and crucially do not fundamentally break the relationship between ε_p values and atmospheric CO_2 concentration. However if this is not the case, and the relationship between ε_p values and atmospheric CO_2 concentration fails at Pleistocene levels of atmospheric CO_2 then Pleistocene records cannot be used to develop corrections of $CO_{2(\varepsilon_p-\mathrm{alk})}$ to be applied throughout the Cenozoic. If, as suggested by the analyses presented here, CCMs *only* act at low $[CO_2]_{(aq)}$, and largely only in conditions prevalent throught the late Pliocene and Pleistocene, it is plausible that corrections based on Pleistocene records could overcompensate for CCMs in the rest of the Cenozoic, when the assumption of passive carbon uptake inherent in $CO_{2(\varepsilon_p-\mathrm{alk})}$ as traditionally applied may still be valid.

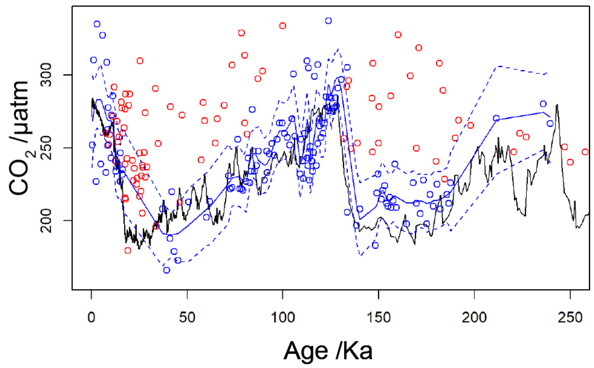

Figure 9. Revised compilation of Pleistocene $CO_{2(\varepsilon_p-\mathrm{alk})}$ vs ice core records. The compiled published records (Table 1) are shown as circles, coloured red where $[CO_2]_{(aq)-\mathrm{predicted}}$ is below a threshold of 7 $\mu mol L^{-1}$, and blue where $[CO_2]_{(aq)-\mathrm{predicted}} > 7$ $\mu mol L^{-1}$. The solid blue line is a loess filter (span 0.1) through the $[CO_2]_{(aq)-\mathrm{predicted}} > 7$ $\mu mol L^{-1}$ values, with 95 % confidence intervals (dashed blue line). The black line is the ice core compilation of Bereiter et al. (2015) (Table 2).

5 Conclusions

Reconstructions of past atmospheric CO_2 concentration with proxy tools like $CO_{2(\varepsilon_p-\mathrm{alk})}$ are critical for understanding how the Earth's climate system operates, as long as the tools used can be relied upon to be accurate and precise. This re-analysis of existing Pleistocene $CO_{2(\varepsilon_p-\mathrm{alk})}$ records reveals that below a critical threshold of $[CO_2]_{(aq)}$ of 7 $\mu mol L^{-1}$ the relationship between $\delta^{13}C_{\mathrm{alkenone}}$ and atmospheric CO_2 concentration breaks down, plausibly because below this threshold haptophytes are able to actively take up carbon using CCMs in order to satisfy metabolic demand.

Although reconstructing the low levels of atmospheric CO_2 concentration in the Pleistocene glacials and areas of the global ocean where $[CO_2]_{(aq)}$ is less than 7 $\mu mol L^{-1}$ will be impossible, for much of the Cenozoic, the $CO_{2(\varepsilon_p-\mathrm{alk})}$ proxy retains utility. If care is taken to avoid regions and oceanographic settings where $[CO_2]_{(aq)}$ is expected to be abnormally low, $CO_{2(\varepsilon_p-\mathrm{alk})}$ remains an important and useful proxy to understand the Earth system.

Code and data availability. This paper relies exclusively on previously published data, available with the original papers and in publicly available repositories. An R notebook supplement is available alongside this manuscript, along with datafiles which allow full replication of all analyses performed.

Author contributions. MPSB conceived the study, designed the methodology, analysed the data, prepared the figures and wrote the manuscript (conceptualization, formal analysis, investigation, methodology, vizualization, writing - original draft, review and editing)

Competing interests. MPSB declares that he has no conflict of interest

Acknowledgements. I am grateful to Gavin Foster and Tom Chalk for frequent and stimulating discussions on alkenone paleobarometry. I thank all authors who made full datasets available online. I thank Kirsty Edgar for comments on various drafts, and the two anonymous reviewers whose comments greatly improved this manuscript.

References

Ahn, J. and Brook, E. J.: Siple Dome ice reveals two modes of millennial CO2 change during the last ice age, Nature Communications, 5, 3723, http://dx.doi.org/10.1038/ncomms4723, 2014.

Anagnostou, E., John, E. H., Edgar, K. M., Foster, G. L., Ridgwell, A., Inglis, G. N., Pancost, R. D., Lunt, D. J., and Pearson, P. N.: Changing atmospheric CO2 concentration was the primary driver of early Cenozoic climate, Nature, 533, 380–384, https://doi.org/10.1038/nature17423, http://www.nature.com/doifinder/10.1038/nature17423, 2016.

Andersen, N., Miiller, P. J., Kirsf, G., and Schneider, R. R.: Alkenone delta-13C as a proxy for past pCO2 in surface waters: Results from the Late Quarternary Angola Current, 1999.

Antonov, J. I., Seidov, D., Boyer, T. P., Locarnini, R. A., Mishonov, A. V., Garcia, H. E., Baranova, O. K., Zweng, M. M., and Johnson, D. R.: World Ocean Atlas 2009, Volume 2: Salinity, https://doi.org/10.1182/blood-2011-06-357442, 2010.

Badger, M. P., Lear, C. H., Pancost, R. D., Foster, G. L., Bailey, T. R., Leng, M. J., and Abels, H. a.: CO2 drawdown following the middle Miocene expansion of the Antarctic Ice Sheet, Paleoceanography, 28, 42–53, https://doi.org/10.1002/palo.20015, 2013a.

Badger, M. P., Foster, G. L., Chalk, T. B., Gibbs, S. J., Badger, M. P. S., Pancost, R. D., Schmidt, D. N., Sexton, P. F., Mackensen, A., Bown, P. R., and Pälike, H.: Insensitivity of alkenone carbon isotopes to atmospheric CO2 at low to moderate CO2 levels, Climate of the Past, 15, 539–554, https://doi.org/10.5194/cp-2018-152, 2019.

Badger, M. P. S., Schmidt, D. N., Mackensen, A., and Pancost, R. D.: High-resolution alkenone palaeobarometry indicates relatively stable pCO(2) during the Pliocene (3.3-2.8 Ma)., Philosophical transactions. Series A, Mathematical, physical, and engineering sciences, 371, 20130 094, https://doi.org/10.1098/rsta.2013.0094, http://www.ncbi.nlm.nih.gov/pubmed/24043868, 2013b.

Bae, S. W., Lee, K. E., and Kim, K.: Use of carbon isotopic composition of alkenone as a CO2 proxy in the East Sea/Japan Sea, Continental Shelf Research, 107, 24–32, https://doi.org/10.1016/j.csr.2015.07.010, https://www.sciencedirect.com/science/article/pii/S0278434315300133?via{%}3Dihubhttps://linkinghub.elsevier.com/retrieve/pii/S0278434315300133, 2015.

Beerling, D. J. and Royer, D. L.: Convergent Cenozoic CO2 history, Nature Geoscience, 4, 418–420, https://doi.org/10.1038/ngeo1186, http://dx.doi.org/10.1038/ngeo1186, 2011.

Bereiter, B., Lüthi, D., Siegrist, M., Schüpbach, S., Stocker, T. F., and Fischer, H.: Mode change of millennial CO2 variability during the last glacial cycle associated with a bipolar marine carbon seesaw, Proceedings of the National Academy of Sciences, 109, 9755–9760, https://doi.org/10.1073/pnas.1204069109, http://www.pnas.org/content/109/25/9755.abstract, 2012.

Bereiter, B., Eggleston, S., Schmitt, J., Nehrbass-Ahles, C., Stocker, T. F., Fischer, H., Kipfstuhl, S., and Chappellaz, J.: Revision of the EPICA Dome C CO 2 record from 800 to 600 kyr before present, Geophysical Research Letters, 42, 542–549, https://doi.org/10.1002/2014GL061957, http://doi.wiley.com/10.1002/2014GL061957, 2015.

Bidigare, R., Fluegge, A., Freeman, K. H., Hanson, K., Hayes, J. M., Hollander, D., Jasper, J. P., King, L. L., Laws, E., Milder, J., Millero, F. J., Pancost, R., Popp, B. N., Steinberg, P., and Wakeham, S. G.: Consistent fractionation of 13C in nature and in the laboratory: Growth-rate effects in some haptophyte algae, Global Biogeochemical Cycles, 11, 279–292, http://onlinelibrary.wiley.com/doi/10.1029/96GB03939/full, 1997.

Bolton, C. T. and Stoll, H. M.: Late Miocene threshold response of marine algae to carbon dioxide limitation., Nature, 500, 558–62, https://doi.org/10.1038/nature12448, http://www.ncbi.nlm.nih.gov/pubmed/23985873, 2013.

Bolton, C. T., Stoll, H. M., and Mendez-Vicente, A.: Vital effects in coccolith calcite: Cenozoic climate- p CO 2 drove the diversity of carbon acquisition strategies in coccolithophores?, Paleoceanography, 27, n/a–n/a, https://doi.org/10.1029/2012PA002339, http://doi.wiley.com/10.1029/2012PA002339, 2012.

Brassell, S., Eglinton, G., and Marlowe, I.: Molecular stratigraphy: a new tool for climatic assessment, Nature, 320, 129–133, http://www.geology.fsu.edu/{~}odom/orbitalforcingstratigraphy/Brassell-Original{_}Alkenone{_}Paper-Na86.pdf, 1986.

Cassar, N., Laws, E. a., and Popp, B. N.: Carbon isotopic fractionation by the marine diatom Phaeodactylum tricornutum under nutrient- and light-limited growth conditions, Geochimica et Cosmochimica Acta, 70, 5323–5335, https://doi.org/10.1016/j.gca.2006.08.024, http://linkinghub.elsevier.com/retrieve/pii/S0016703706020084, 2006.

Conte, M. H., Volkman, J. K., and Eglinton, G.: Lipid biomarkers of the Haptophyta, in: The Haptophyte algae, edited by Green, J. and Leadbeater, B., pp. 351–377, Oxford University Press, UK, 1994.

Farrimond, P., Eglinton, G., and Brassell, S. C.: Alkenones in Cretaceous black shales, Blake-Bahama Basin, western North Atlantic, Organic Geochemistry, 10, 897–903, https://doi.org/10.1016/S0146-6380(86)80027-4, 1986.

Foster, G. L., Lear, C. H., and Rae, J. W. B.: The evolution of pCO2, ice volume and climate during the middle Miocene, Earth and Planetary Science Letters, 341-344, 243–254, https://doi.org/10.1016/j.epsl.2012.06.007, http://linkinghub.elsevier.com/retrieve/pii/S0012821X12002919, 2012.

Foster, G. L., Royer, D. L., and Lunt, D. J.: Future climate forcing potentially without precedent in the last 420 million years, Nature Communications, 8, 14 845, https://doi.org/10.1038/ncomms14845, http://www.nature.com/doifinder/10.1038/ncomms14845, 2017.

Garcia, H. E., Locarnini, R. A., Boyer, T. P., Antonov, J. I., Baranova, O. K., Zweng, M. M., Reagan, J. R., and Johnson, D. R.: World Ocean Atlas 2013, Volume 4 : Dissolved Inorganic Nutrients (phosphate, nitrate, silicate), 2013.

Gradstein, F., Ogg, J., Schmitz, M., and Ogg, G.: The Geologic Time Scale 2012, Elsevier, 1 edn., 2012.

Jasper, J. and Hayes, J.: A carbon isotope record of CO2 levels during the late Quaternary, Nature, 347, 462–464, http://www.nature.com/nature/journal/v347/n6292/abs/347462a0.html, 1990.

Jasper, J., Hayes, J., Mix, A., and Prahl, F.: Photosynthetic fractionation of 13C and concentrations of dissolved CO2 in the central equatorial Pacific during the last 255,000 years, Paleoceanography, 9, 781–798, http://onlinelibrary.wiley.com/doi/10.1029/94PA02116/full, 1994.

Kürschner, W. M., Kvacek, Z., and Dilcher, D. L.: The impact of Miocene atmospheric carbon dioxide fluctuations on climate and the evolution, Proceedings of the National Academy of Sciences of the United States of America, 105, 449–453, 2008.

Laws, E., Popp, B., Bidigare, R., Kennicutt, M., and Macko, S.: Dependence of phytoplankton carbon isotopic composition on growth rate and [CO 2) aq: Theoretical considerations and experimental, Geochimica et Cosmochimica Acta, 59, 1131–1138, http://www.sciencedirect.com/science/article/pii/0016703795000304, 1995.

Laws, E. a., Bidigare, R. R., and Popp, B. N.: Effect of growth rate and CO2 concentration on carbon isotopic fractionation by the marine diatom Phaeodactylum tricornutum, Limnology and Oceanography, 42, 1552–1560, https://doi.org/10.4319/lo.1997.42.7.1552, http://doi.wiley.com/10.4319/lo.1997.42.7.1552, 1997.

Laws, E. a., Popp, B. N., Cassar, N., and Tanimoto, J.: 13C discrimination patterns in oceanic phytoplankton: likely influence of CO2 concentrating mechanisms, and implications for palaeoreconstructions, Functional Plant Biology, 29, 323–333, https://doi.org/10.1071/Pp01183, 2002.

Locarnini, R. A., Mishonov, A. V., Antonov, J. I., Boyer, T. P., Garcia, H. E., Baranova, O. K., Zweng, M. M., Paver, C. R., Reagan, J. R., Johnson, D. R., Hamilton, M., and Seidov, D.: World Ocean Atlas 2013. Vol. 1: Temperature., Tech. rep., https://doi.org/10.1182/blood-2011-06-357442, 2013.

MacFarling Meure, C., Etheridge, D., Trudinger, C., Steele, P., Langenfelds, R., van Ommen, T., Smith, A., and Elkins, J.: Law Dome CO2, CH4 and N2O ice core records extended to 2000 years BP, Geophysical Research Letters, 33, L14 810, https://doi.org/10.1029/2006gl026152, http://dx.doi.org/10.1029/2006GL026152, 2006.

Marcott, S. A., Bauska, T. K., Buizert, C., Steig, E. J., Rosen, J. L., Cuffey, K. M., Fudge, T. J., Severinghaus, J. P., Ahn, J., Kalk, M. L., McConnell, J. R., Sowers, T., Taylor, K. C., White, J. W. C., and Brook, E. J.: Centennial-scale changes in the global carbon cycle during the last deglaciation, Nature, 514, 616–619, http://dx.doi.org/10.1038/nature13799, 2014.

Marlowe, I., Brassell, S., Eglinton, G., and Green, J.: Long-chain alkenones and alkyl alkenoates and the fossil coccolith record of marine sediments, Chemical Geology, 88, 349–375, https://doi.org/10.1016/0009-2541(90)90098-R, http://linkinghub.elsevier.com/retrieve/pii/000925419090098R, 1990.

Martínez-Botí, M. A., Foster, G. L., Chalk, T. B., Rohling, E. J., Sexton, P. F., Lunt, D. J., Pancost, R. D., Badger, M. P., and Schmidt, D. N.: Plio-Pleistocene climate sensitivity evaluated using high-resolution CO2 records, Nature, 518, 49–54, https://doi.org/10.1038/nature14145, http://dx.doi.org/10.1038/nature14145, 2015.

Monnin, E., Indermuhle, A., Dallenbach, A., Fluckiger, J., Stauffer, B., Stocker, T. F., Raynaud, D., and Barnola, J. M.: Atmospheric CO2 concentrations over the last glacial termination, Science, 291, 112–114, https://doi.org/10.1126/science.291.5501.112, 2001.

Monnin, E., Steig, E. J., Siegenthaler, U., Kawamura, K., Schwander, J., Stauffer, B., Stocker, T. F., Morse, D. L., Barnola, J.-M., Bellier, B., Raynaud, D., and Fischer, H.: Evidence for substantial accumulation rate variability in Antarctica during the Holocene, through synchronization of CO2 in the Taylor Dome, Dome C and DML ice cores, Earth and Planetary Science Letters, 224, 45–54, https://doi.org/10.1016/j.epsl.2004.05.007, http://linkinghub.elsevier.com/retrieve/pii/S0012821X04003115, 2004.

Mook, W. G., Bommerson, J. C., and Staverman, W. H.: Carbon isotope fractionation between dissolved bicarbonate and gaseous carbon dioxide, Earth and Planetary Science Letters, 22, 169–176, https://doi.org/10.1016/0012-821X(74)90078-8, 1974.

Pagani, M., Freeman, K., and Arthur, M.: Late Miocene atmospheric CO2 concentrations and the expansion of C4 grasses, Science, 285, 876–879, http://www.sciencemag.org/content/285/5429/876.short, 1999.

Pagani, M., Zachos, J. C., Freeman, K. H., Tipple, B., and Bohaty, S.: Marked decline in atmospheric carbon dioxide concentrations during the Paleogene., Science (New York, N.Y.), 309, 600–603, https://doi.org/10.1126/science.1110063, http://www.ncbi.nlm.nih.gov/pubmed/15961630, 2005.

Pagani, M., Liu, Z., LaRiviere, J., and Ravelo, A. C.: High Earth-system climate sensitivity determined from Pliocene carbon dioxide concentrations, Nature Geoscience, 3, 27–30, https://doi.org/10.1038/ngeo724, http://www.nature.com/doifinder/10.1038/ngeo724, 2009.

Pagani, M., Huber, M., Liu, Z., Bohaty, S. M., Henderiks, J., Sijp, W., Krishnan, S., and DeConto, R. M.: The role of carbon dioxide during the onset of Antarctic glaciation., Science (New York, N.Y.), 334, 1261–4, https://doi.org/10.1126/science.1203909, http://www.ncbi.nlm.nih.gov/pubmed/22144622, 2011.

Palmer, M. R., Brummer, G. J., Cooper, M. J., Elderfield, H., Greaves, M. J., Reichart, G. J., Schouten, S., and Yu, J. M.: Multi-proxy reconstruction of surface water pCO2 in the northern Arabian Sea since 29ka, Earth and Planetary Science Letters, 295, 49–57, https://doi.org/10.1016/j.epsl.2010.03.023, http://linkinghub.elsevier.com/retrieve/pii/S0012821X10002049, 2010.

Pearson, P. N., Foster, G. L., and Wade, B. S.: Atmospheric carbon dioxide through the Eocene-Oligocene climate transition., Nature, 461, 1110–1113, https://doi.org/10.1038/nature08447, http://www.ncbi.nlm.nih.gov/pubmed/19749741, 2009.

Petit, J. R., Jouzel, J., Raynaud, D., Barkov, N. I., Barnola, J.-M., Basile, I., Bender, M., Chappellaz, J., Davis, M., Delaygue, G., Delmotte, M., Kotlyakov, V. M., Legrand, M., Lipenkov, V. Y., Lorius, C., Pepin, K., Ritz, C., Saltzman, E., and Stievenard, M.: Climate and atmospheric history of the past 420,000 years from the Vostok ice core, Antarctica, Nature, 399, 429–436, http://www.nature.com/nature/journal/v399/n6735/abs/399429a0.html, 1999.

Popp, B., Laws, E., Bidigare, R., Dore, J., Hanson, K., and Wakeham, S. G.: Effect of phytoplankton cell geometry on carbon isotopic fractionation, Geochimica et Cosmochimica Acta, 62, 67–77, http://www.sciencedirect.com/science/article/pii/S0016703797003335, 1998.

R Core Team: R: A language and environment for statistical computing, https://www.r-project.org/, 2020.

Raffi, I., Backman, J., Fornaciari, E., Pälike, H., Rio, D., Lourens, L., and Hilgen, F.: A review of calcareous nannofossil astrobiochronology encompassing the past 25 million years☆, Quaternary Science Reviews, 25, 3113–3137, https://doi.org/10.1016/j.quascirev.2006.07.007, http://linkinghub.elsevier.com/retrieve/pii/S0277379106002320, 2006.

Rechka, J. and Maxwell, J.: Characterisation of alkenone temperature indicators in sediments and organisms, Organic Geochemistry, 13, 727–734, http://www.sciencedirect.com/science/article/pii/0146638088900940, 1987.

Reinfelder, J. R.: Carbon concentrating mechanisms in eukaryotic marine phytoplankton., Annual review of marine science, 3, 291–315, https://doi.org/10.1146/annurev-marine-120709-142720, http://www.annualreviews.org/doi/full/10.1146/annurev-marine-120709-142720, 2011.

Riebesell, U., Revill, A. T., Holdsworth, D. G., and Volkman, J. K.: The effects of varying CO2 concentration on lipid composition and carbon isotope fractionation in Emiliania huxleyi, Geochimica et Cosmochimica Acta, 64, 4179–4192, https://doi.org/10.1016/S0016-7037(00)00474-9, http://linkinghub.elsevier.com/retrieve/pii/S0016703700004749, 2000.

Riebesell, U., Schulz, K. G., Bellerby, R. G., Botros, M., Fritsche, P., Meyerhöfer, M., Neill, C., Nondal, G., Oschlies, A., Wohlers, J., and Zöllner, E.: Enhanced biological carbon consumption in a high CO2 ocean, Nature, 450, 545–548, https://doi.org/10.1038/nature06267, 2007.

Romanek, C. S., Grossman, E. L., and Morse, J. W.: Carbon isotopic fractionation in synthetic aragonite and calcite: Effects of temperature and precipitation rate, Geochimica et Cosmochimica Acta, 56, 419–430, https://doi.org/10.1016/0016-7037(92)90142-6, http://linkinghub.elsevier.com/retrieve/pii/0016703792901426, 1992.

Rost, B., Riebesell, U., Burkhardt, S., and Sültemeyer, D.: Carbon acquisition of bloom-forming marine phytoplankton, Limnology and Oceanography, 48, 55–67, https://doi.org/10.4319/lo.2003.48.1.0055, 2003.

RStudio Team: RStudio: Integrated Development for R, http://www.rstudio.com/, 2020.

Rubino, M., Etheridge, D. M., Trudinger, C. M., Allison, C. E., Battle, M. O., Langenfelds, R. L., Steele, L. P., Curran, M., Bender, M., White, J. W. C., Jenk, T. M., Blunier, T., and Francey, R. J.: A revised 1000 year atmospheric δ13C-CO2 record from Law Dome and South Pole, Antarctica, Journal of Geophysical Research: Atmospheres, 118, 8482–8499, https://doi.org/10.1002/jgrd.50668, http://dx.doi.org/10.1002/jgrd.50668, 2013.

Schneider, R., Schmitt, J., Köhler, P., Joos, F., and Fischer, H.: A reconstruction of atmospheric carbon dioxide and its stable carbon isotopic composition from the penultimate glacial maximum to the last glacial inception, Climate of the Past, 9, 2507–2523, 2013.

Sosdian, S. M., Greenop, R., Hain, M. P., Foster, G. L., Pearson, P. N., and Lear, C. H.: Constraining the evolution of Neogene ocean carbonate chemistry using the boron isotope pH proxy, Earth and Planetary Science Letters, 498, 362–376, https://doi.org/10.1016/j.epsl.2018.06.017, https://www.sciencedirect.com/science/article/pii/S0012821X1830356X, 2018.

Stoll, H. M., Guitian, J., Hernandez-Almeida, I., Mejia, L. M., Phelps, S., Polissar, P., Rosenthal, Y., Zhang, H., and Ziveri, P.: Upregulation of phytoplankton carbon concentrating mechanisms during low CO 2 glacial periods and implications for the phytoplankton pCO 2 proxy, Quaternary Science Reviews, 208, 1–20, https://doi.org/10.1016/j.quascirev.2019.01.012, https://doi.org/10.1016/j.quascirev.2019.01.012, 2019.

Super, J. R., Thomas, E., Pagani, M., Huber, M., Brien, C. O., and Hull, P. M.: North Atlantic temperature and pCO2 coupling in the early-middle Miocene, Geology, 46, 519–522, https://doi.org/https://doi.org/10.1130/G40228.1, https://pubs.geoscienceworld.org/gsa/geology/article/46/6/519/530691/North-Atlantic-temperature-and-pCO2-coupling-in, 2018.

Takahashi, T., Sutherland, S. C., Wanninkhof, R., Sweeney, C., Feely, R. a., Chipman, D. W., Hales, B., Friederich, G., Chavez, F., Sabine, C., Watson, A., Bakker, D. C. E., Schuster, U., Metzl, N., Yoshikawa-Inoue, H., Ishii, M., Midorikawa, T., Nojiri, Y., Körtzinger, A., Steinhoff, T., Hoppema, M., Olafsson, J., Arnarson, T. S., Tilbrook, B., Johannessen, T., Olsen, A., Bellerby, R., Wong, C. S., Delille, B., Bates, N. R., and de Baar, H. J. W.: Climatological mean and decadal change in surface ocean pCO2, and net sea–air CO2 flux over the global oceans, Deep Sea Research Part II: Topical Studies in Oceanography, 56, 554–577, https://doi.org/10.1016/j.dsr2.2008.12.009, http://linkinghub.elsevier.com/retrieve/pii/S0967064508004311, 2009.

Takahashi, T., Sutherland, S. C., Chipman, D. W., Goddard, J., Newberber, T., and Sweeney, C.: Climatological Distributions of pH, pCO2, Total CO2, Alkalinity, and CaCO3 Saturation in the Global Surface Ocean, in: Climatological Distributions of pH, pCO2, Total CO2, Alkalinity, and CaCO3 Saturation in the Global Surface Ocean. ORNL/CDIAC-160, NDP-094, Carbon Dioxide Information Analysis Center, Oak Ridge National Laboratory, U.S. Department of Energy, Oak Ridge, Tennessee, https://doi.org/10.3334/CDIAC/OTG.NDP094, 2014.

Tchernov, D., Silverman, J., Luz, B., Reinhold, L., and Kaplan, A.: Massive light-dependent cycling of inorganic carbon between oxygenic photosynthetic microorganisms and their surroundings, Photosynthesis Research, 77, 95–103, https://doi.org/10.1023/A:1025869600935, 2003.

Trimborn, S., Langer, G., and Rost, B.: Effect of varying calcium concentrations and light intensities on calcification and photosynthesis in Emiliania huxleyi, Limnology and Oceanography, 52, 2285–2293, https://doi.org/10.4319/lo.2007.52.5.2285, 2007.

Volkman, J. K.: Ecological and environmental factors affecting alkenone distributions in seawater and sediments, Geochemistry, Geophysics, Geosystems, 1, n/a–n/a, https://doi.org/10.1029/2000GC000061, http://doi.wiley.com/10.1029/2000GC000061, 2000.

Weiss, R. F.: The solubility of nitrogen, oxygen and argon in water and seawater, Deep-Sea Research and Oceanographic Abstracts, 17, 721–735, https://doi.org/10.1016/0011-7471(70)90037-9, 1970.

Weiss, R. F.: Carbon dioxide in water and seawater: the solubility of a non-ideal gas, Marine Chemistry, 2, 203–215, 1974.

Wessel, P. and Smith, W. H. F.: A global, self-consistent, hierarchical, high-resolution shoreline database, Journal of Geophysical Research: Solid Earth, 101, 8741–8743, https://doi.org/10.1029/96JB00104, http://doi.wiley.com/10.1029/96JB00104, 1996.

Wessel, P., Luis, J. F., Uieda, L., Scharroo, R., Wobbe, F., Smith, W. H. F., and Tian, D.: The Generic Mapping Tools Version 6, Geochemistry, Geophysics, Geosystems, 20, 5556–5564, https://doi.org/10.1029/2019GC008515, https://onlinelibrary.wiley.com/doi/abs/10.1029/2019GC008515, 2019.

Zhang, Y. G., Pagani, M., Liu, Z., Bohaty, S. M., and Deconto, R.: A 40-million-year history of atmospheric CO(2)., Philosophical transactions. Series A, Mathematical, physical, and engineering sciences, 371, 20130 096, https://doi.org/10.1098/rsta.2013.0096, http://www.ncbi.nlm.nih.gov/pubmed/24043869, 2013.

Zhang, Y. G., Pearson, A., Benthien, A., Dong, L., Huybers, P., Liu, X., and Pagani, M.: Refining the alkenone-pCO2 method I: Lessons from the Quaternary glacial cycles, Geochimica et Cosmochimica Acta, 260, 177–191, https://doi.org/10.1016/j.gca.2019.06.032, https://doi.org/10.1016/j.gca.2019.06.032, 2019.

Zhang, Y. G., Henderiks, J., and Liu, X.: Refining the alkenone-pCO2 method II: Towards resolving the physiological parameter 'b', Geochimica et Cosmochimica Acta, 281, 118–134, https://doi.org/10.1016/j.gca.2020.05.002, https://doi.org/10.1016/j.gca.2020.05.002, 2020.

Zondervan, I., Rost, B., and Riebesell, U.: Effect of CO2 concentration on the PIC/POC ratio in the coccolithophore Emiliania huxleyi grown under light-limiting conditions and different daylengths, Journal of Experimental Marine Biology and Ecology, 272, 55–70, https://doi.org/10.1016/S0022-0981(02)00037-0, https://linkinghub.elsevier.com/retrieve/pii/S0022098102000370, 2002.